Stem Cell Reports
Article

OPEN ACCESS

Intercellular Adhesion-Dependent Cell Survival and ROCK-Regulated Actomyosin-Driven Forces Mediate Self-Formation of a Retinal Organoid

Albert Lowe,[1] Raven Harris,[1] Punita Bhansali,[1] Ales Cvekl,[1,2] and Wei Liu[1,2,*]
[1]Department of Genetics
[2]Department of Ophthalmology and Visual Sciences
Albert Einstein College of Medicine, Bronx, NY 10461, USA
*Correspondence: wei.liu@einstein.yu.edu
http://dx.doi.org/10.1016/j.stemcr.2016.03.011

SUMMARY

In this study we dissected retinal organoid morphogenesis in human embryonic stem cell (hESC)-derived cultures and established a convenient method for isolating large quantities of retinal organoids for modeling human retinal development and disease. Epithelialized cysts were generated via floating culture of clumps of Matrigel/hESCs. Upon spontaneous attachment and spreading of the cysts, patterned retinal monolayers with tight junctions formed. Dispase-mediated detachment of the monolayers and subsequent floating culture led to self-formation of retinal organoids comprising patterned neuroretina, ciliary margin, and retinal pigment epithelium. Intercellular adhesion-dependent cell survival and ROCK-regulated actomyosin-driven forces are required for the self-organization. Our data supports a hypothesis that newly specified neuroretina progenitors form characteristic structures in equilibrium through minimization of cell surface tension. In long-term culture, the retinal organoids autonomously generated stratified retinal tissues, including photoreceptors with ultrastructure of outer segments. Our system requires minimal manual manipulation, has been validated in two lines of human pluripotent stem cells, and provides insight into optic cup invagination in vivo.

INTRODUCTION

Stem cell-derived retinal organoid culture is a promising tool for studying human retinal development and disease (Lancaster and Knoblich, 2014). The growth of retinal organoids from human embryonic stem cells (hESCs) or human induced pluripotent stem cells (hiPSCs) mimics the process of retinal development in vivo. Retinal organoids derived from patient-specific hiPSCs are used in disease modeling and drug testing.

Retinal development in vivo is a multi-step process of cell-fate specification that is regulated by transcription factors, signal transduction molecules, and cell surface molecules. Extracellular matrix (ECM)-mediated epithelialization of the epiblast and the eye field are critical events prior to retinal specification (Bedzhov and Zernicka-Goetz, 2014; Coucouvanis and Martin, 1995; Ivanovitch et al., 2013). Early retinal progenitor cells (RPCs) in the eye field express key transcription factors, including SIX3, RAX, PAX6, and OTX2 (Liu et al., 2010). The eye field evaginates to form the optic vesicle, which later invaginates to form the optic cup with RPCs for neuroretina (NR; $VSX2^{+}$ $PAX6^{moderate}$) in the inner layer and progenitors for retinal pigment epithelium (RPE; $MITF^{+}$ $PAX6^{high}$) in the outer layer (Liu et al., 2010). Ciliary margin (CM) is then specified at NR-RPE boundaries.

Tissue formation relies on cell-cell and cell-ECM adhesions via transmembrane proteins to transduce signals between the intra- and extracellular domains that are linked to actomyosin networks and cell-cell/ECM adhesions, respectively (Jockusch et al., 1995). Disruption of cell-ECM adhesions by cell detachment leads to anoikis (a specific type of apoptosis) (Frisch and Francis, 1994). Similarly, disruption of cell-cell adhesions by inactivation of tight junction (TJ) protein TJP1 or adherens junction (AJ) protein CDH2 causes apoptosis (Katsuno et al., 2008; Oliver et al., 2013; Wheelock et al., 2008). Related spatially and functionally, TJs and AJs are highly dynamic in morphogenesis and are involved in the regulation of apicobasal polarity (Rothen-Rutishauser et al., 2002). The cadherin ring of the AJs couples with a nearby bundle of F-actin to support morphogenesis of epithelial cells.

Numerous morphogenetic events are explained by the cell surface tension model. In equilibrium, surface tension is minimized via coordinated forces generated by cell surface tension and actomyosin-mediated cortical tension, resulting in cell sorting and self-organization (Beysens et al., 2000; Heisenberg and Bellaiche, 2013; Lecuit and Lenne, 2007; Steinberg, 1963). Rho kinase (ROCK) regulates actomyosin networks and cell polarity (Amano et al., 2010). Myosin activation and cell contraction depend on the phosphorylation of myosin regulatory light chains (pMYL) by apical ROCK.

Significant progress has been made in generating retinal structures from hESC or hiPSC cultures in which a regime of extrinsic factors with or without Matrigel are used (Boucherie et al., 2013; Lamba et al., 2009; Meyer et al., 2011; Nakano et al., 2012; Reichman et al., 2014; Zhong et al., 2014; Zhu et al., 2013). However, mechanistic understanding of the in vitro process is only beginning. Deeper

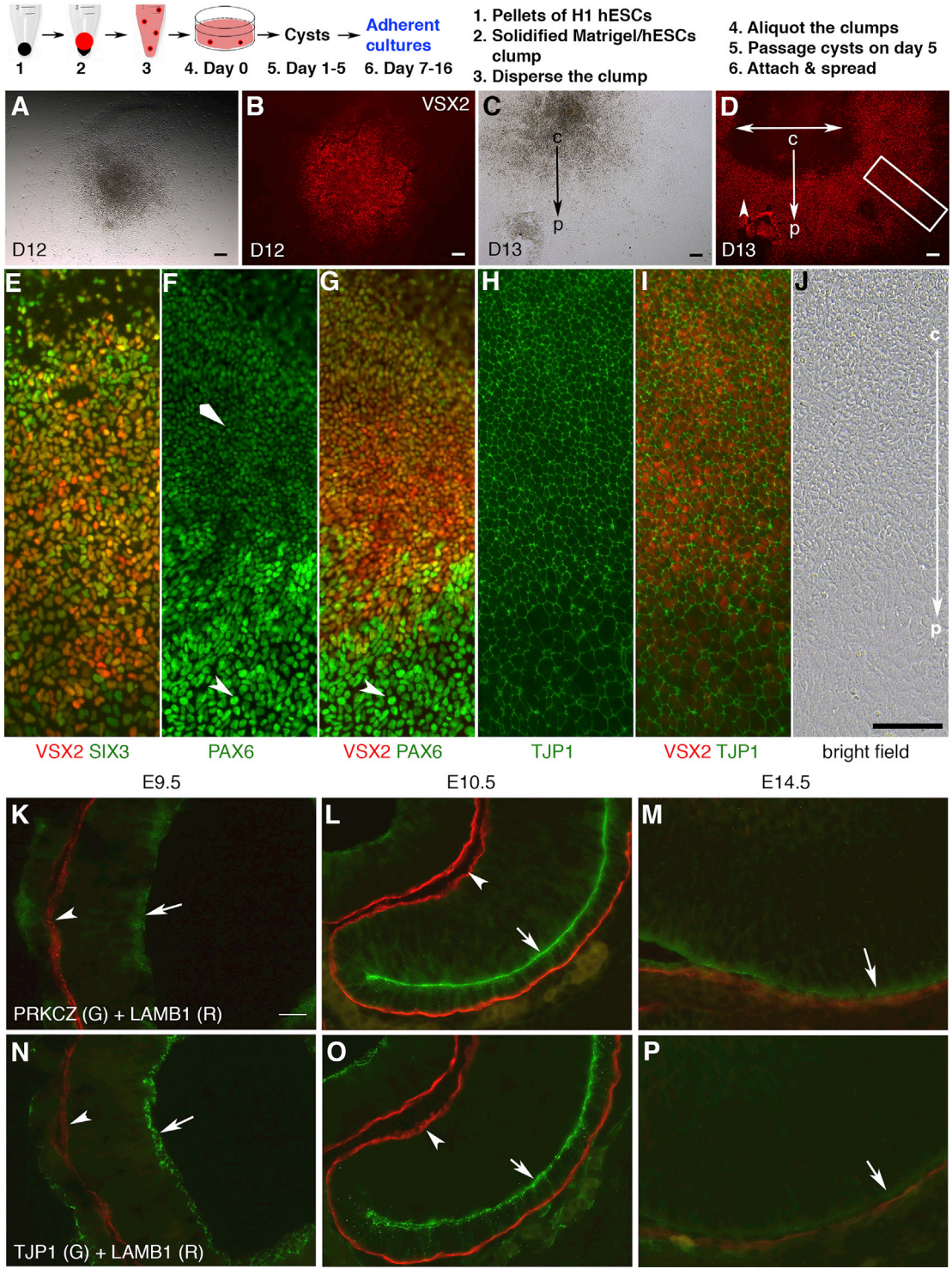

Figure 1. VSX2^{+} RPCs and PAX6^{high} RPE Progenitors Form Patterned Epithelial Monolayer Sheets upon Spontaneous Attachment and Spreading of the Cysts

(A–D) In a procedure shown in the scheme, the cysts spontaneously attached to a culture surface and spread, forming monolayer colonies. Adherent cultures on days (D) 12–16 were used for immunocytochemistry. In a well of 24-well plates, 4–7 patches of VSX2^{+} RPCs were found (n = 5/5, independent wells). VSX2^{+} RPCs assembled as a disk on D12 (B, bright field in A) and as a ring on D13 (arrowhead in D, bright field in C). Double-headed arrow (D) indicates the spreading of VSX2^{+} RPCs.

(legend continued on next page)

insight into retinal differentiation in vitro will help develop a better procedure for generating retinal cells in stem cell-based research.

Here we dissected retinal organoid morphogenesis in hESC cultures and established a Dispase-mediated method for isolating large quantities of retinal organoids comprising patterned NR, RPE, and CM. Our findings demonstrate that intercellular adhesion-dependent cell survival and ROCK-regulated actomyosin-driven forces are required for self-organization of retinal organoids, and support a hypothesis that newly specified VSX2$^+$ RPCs form characteristic structures in equilibrium via minimization of cell surface tension. In long-term culture, the retinal organoids generate stratified retinal tissues, including photoreceptors that contain the ultrastructure of outer segments. Our system requires minimal manual manipulation, has been validated in two lines of hPSCs, and thus has multiple applications in modeling human retinal development and disease.

RESULTS

Efficient Generation of Polarized Early RPCs via Matrigel-Aided Cyst Formation

The pivotal roles of ECM in the epithelialization of mouse epiblast (Bedzhov and Zernicka-Goetz, 2014; Coucouvanis and Martin, 1995) and zebrafish eye-field cells (Ivanovitch et al., 2013) suggest that Matrigel/ECM is important for the epithelialization of hESCs toward retinal differentiation. We developed a procedure for retinal differentiation via floating culture of Matrigel/hESC clumps (Figure S1). Small sheets of H1 hESCs were suspended in Matrigel for gelification and then the clump of Matrigel/hESCs was gently dispersed for floating culture. Numerous epithelialized cysts with a single lumen formed on day 1. The cysts generated with our method grew in pliable Matrigel instead of in a stiffened Matrigel layer on the culture surface (Zhu et al., 2013). Without three-dimensional (3D) contact with Matrigel, most cells died and the few surviving cells formed solid cell masses without any visible lumen (Figures S1C and S1E), suggesting that the 3D contact promoted cell survival and epithelialization.

Cells in the cysts gradually differentiated into polarized early RPCs. On day 5, while residual expression of pluripotency marker POU5F1 (OCT4) persisted, anterior neuroectoderm and eye-field marker SIX3 (Liu et al., 2010) was moderately expressed, and eye-field markers RAX and PAX6 were weakly expressed. POU5F1 was downregulated on day 7 and undetectable by day 10 (data not shown). On day 10, SIX3, PAX6, RAX, and OTX2 were expressed in most cells in the cysts (Figures S1F–S1I). Variable expression levels of SIX3 and PAX6 indicated heterogeneity of the cysts (Figures S1F and S1G). On day 13, optic cup marker VSX2 emerged in a few cells (Figure S1N). The cells were proliferative as indicated by KI67 and pH3 (data not shown). Importantly, the cells were coordinately polarized: TJ protein TJP1 (ZO-1) and apical marker PRKCZ (PKCζ) were found at the luminal surface, whereas basal polarity marker LAMB1 (β1-laminin) was at the outer surface (Figures S1J–S1M). Polarized expression of TJP1 in the cells was induced de novo by Matrigel when TJP1 was absent in undifferentiated hESCs (Figures S2A–S2C). The cells self-deposited LAMB1 (Figures S1L and S1M). In sum, 3D contact between hESC aggregates and Matrigel promoted cell survival and coordinated epithelialization, leading to anterior ectoderm/neural plate/early RPCs.

VSX2$^+$ RPCs and PAX6^{high} RPE Progenitors Form Patterned Epithelial Monolayer Sheets after Spontaneous Attachment and Spreading of the Cysts

On day 7, some cysts spontaneously attached to a culture surface and spread, forming monolayer colonies. By day 13 nearly all cysts formed adherent cultures, with a visible center-periphery axis in most colonies (Figures 1 and S2G–S2J). We examined VSX2 expression in the adherent cultures during days 12–16 by immunostaining. In each well of a 24-well plate, 4–7 patches of VSX2-positive (VSX2$^+$) RPCs were found (n = 5/5, independent wells). VSX2$^+$ RPCs assembled as a disc on day 12, and formed a ring-like shape on days 13 and 16 (Figures 1A–1D and S2J), indicating the spreading of VSX2$^+$ RPCs along the center-periphery axis. VSX2$^+$ RPCs sometimes displayed as patches.

In contrast, earlier retinal markers SIX3, PAX6, and OTX2 were broadly expressed (data not shown). VSX2$^+$ RPCs co-expressed SIX3 and PAX6 (Figures 1E–1G). PAX6 was expressed at moderate levels in VSX2$^+$ RPCs and at high levels (PAX6^{high}) in the peripheral VSX2$^-$ cells (Figures 1F and 1G). MITF expression was marginal at this stage (data not shown). The patterning of VSX2$^+$ RPCs and PAX6^{high}

(E–J) Immunostaining of boxed areas in (D). VSX2$^+$ RPCs co-expressed SIX3 and PAX6 (E–G). PAX6^{high} progenitors were peripheral to VSX2$^+$ RPCs, forming a pattern in the center-periphery axis (arrowheads and diamond arrowhead in F and G). Both VSX2$^+$ RPCs and PAX6^{high} progenitors expressed TJP1 (F–J).

(K–P) In mouse retinal development, polarized expression of PRKCZ, TJP1, and LAMB1 peaked in E10.5 RPCs (arrows and arrowheads in K–P).

c, center; p, periphery. Scale bars, 100 μm (A–J) and 20 μm (K–P). See also Figures S1 and S2.

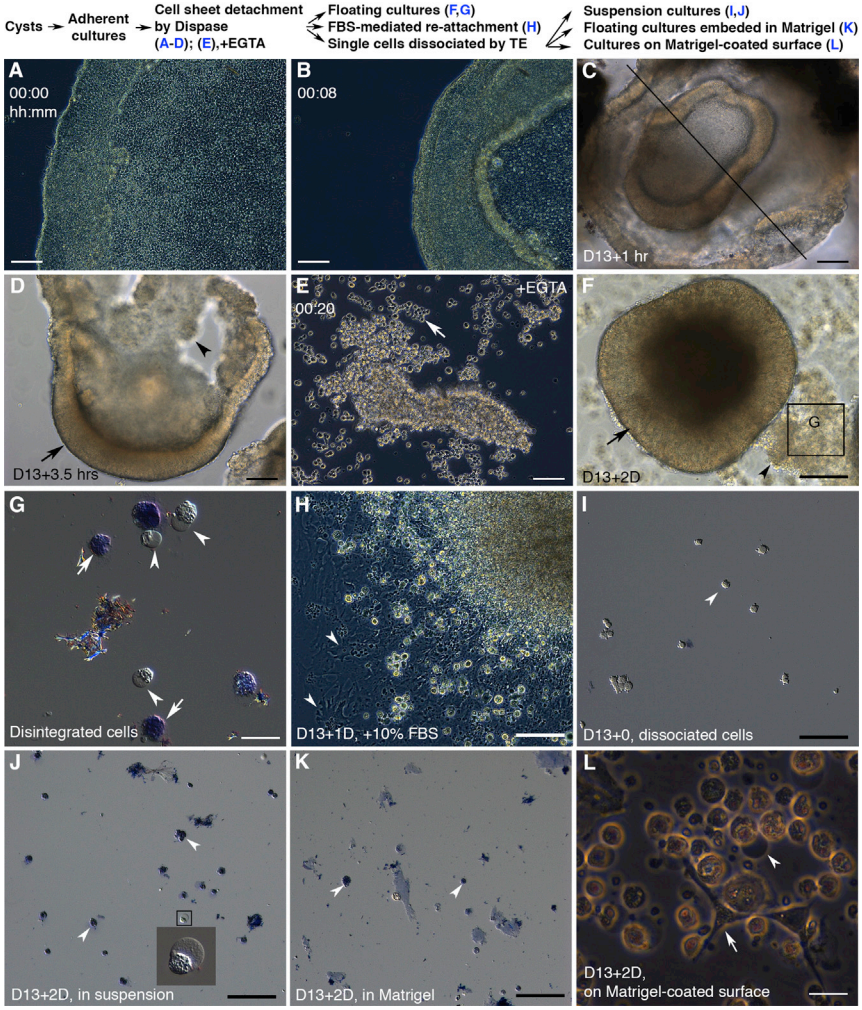

Figure 2. Dispase-Mediated Cell Detachment and Subsequent Floating Culture Lead to Differential Cell Survival via Intercellular Adhesions

(A–L) Treated with Dispase on D13 as indicated in the scheme, the cells with intercellular adhesions lifted up at the edge (A) and then folded up (B–D; sections through the line in C were in Figures 3A and B). EGTA disintegrated the cell sheets (arrow in E). Spheres with a bright ring were visible in 2 days (arrows in D and F). Disintegrated cells (arrowheads in D and F) were either trypan blue positive (arrows in G) or displayed cell blebbing (arrowheads in G), indicative of apoptosis. Serum-mediated reattachment (arrowheads in H) suppressed the apoptosis (H). When the detached cell sheets were dissociated into single cells (arrowhead in I, trypan blue negative) and cultured in suspensions for 2 days, all cells were either trypan blue positive (arrowheads in J) or displayed cell blebbing (inset in J). When the dissociated cells were suspended in Matrigel and cultured as floating clumps, they were trypan blue positive (arrowheads in K). When the dissociated cells were cultured on a Matrigel-coated plate, some cells attached and grew (arrow in L), whereas others remained in suspensions and died (arrowhead in L).

FBS, fetal bovine serum; TE, 0.25% Trypsin/EDTA. Scale bars, 100 μm (A–F, H–K) and 20 μm (G and L). See also Movie S1.

progenitors along the center-periphery axis in the monolayer sheets is reminiscent of dorsoventral patterning in mouse optic vesicles/cups at embryonic day 10 (E10.0) (Liu et al., 2010). Combined with analyses showing the reciprocal positions of NR and RPE (Figures 3B, 3D–3F, 4D, 4F, 4G, and S6I–S6O), the PAX6^{high} cells were identified as RPE progenitors. Importantly, both VSX2^{+} RPCs and PAX6^{high} RPE progenitors expressed TJP1 outlining the cells (Figures 1H–1J). TJP1 expression in VSX2^{+} RPCs in vitro prompted us to examine in vivo expression. In murine retinal development, TJP1 and PRKCZ were expressed at the apical surface of RPCs as well as RPE progenitors, whereas LAMB1 was at the basal surface (Figures 1K–1P). Their peak levels coincided with the peak level of VSX2 expression at E10.5, the stage when the optic cup has formed (Figures 1K–1P and S2N–S2P). Thus, VSX2^{+} RPCs expressed TJP1 in vitro and in vivo, and VSX2^{+} RPCs and PAX6^{high} progenitors formed patterned monolayer sheets in the adherent cultures.

A Dispase-Mediated Method for Isolating the Cell Sheets of VSX2^{+} RPCs and PAX6^{high} RPE Progenitors via Intercellular Adhesion-Dependent Cell Survival

We sought to determine whether VSX2^{+} RPCs in the adherent culture (Figures 1A–1J) could be isolated. After detachment via 0.05% trypsin/EDTA on day 17, spheres of VSX2^{+} epithelium spontaneously formed (data not shown), suggesting that cell detachment causes differential cell behaviors in VSX2^{+} RPCs. After evaluating various methods, we found that Dispase-mediated cell detachment of well-spread monolayers at a time point during days 12–17 enriched VSX2^{+} epithelium and was used hereafter.

Dispase detaches adherent cultures by cleaving fibronectin and collagen IV in ECM-cell adhesions without disrupting intercellular adhesions, and is routinely used for passaging hESCs. Upon Dispase treatment, the monolayer sheets with intercellular adhesions lifted from the edges, quickly contracted, folded up, and eventually detached as open-ended folding cell sheets (Figures 2A–2D;

Movie S1). TJs and AJs disassemble upon EGTA-mediated Ca^{2+}-depletion in MDCK cells (Rothen-Rutishauser et al., 2002). When EGTA was added during Dispase treatment, the cell sheets disintegrated into single cells or small clumps, indicating that the intercellular adhesions holding the cell sheets were Ca^{2+} dependent (Figure 2E). Some Dispase-treated cells became single cells or small clumps even without EGTA, indicative of the absence of intercellular adhesions in these cells. In subsequent floating cultures, the detached cell sheets remodeled into single or fused spheres with a bright ring as seen under an inverted microscope within as early as 2 days (Figure 2F and Movie S2). During this morphogenesis, numerous cells disintegrated and underwent apoptosis (Figures 2F and 2G). The apoptosis was suppressed by serum-mediated reattachment (Figure 2H), indicating that the apoptosis was anoikis (Frisch and Francis, 1994). To examine whether the surviving cells in the spheres were anoikis resistant, we dissociated the detached cell sheets into single cells and cultured them in suspensions. Within 2 days all cells underwent anoikis (Figures 2I and 2J), indicating that the surviving cells in the floating spheres were also sensitive to anoikis and the intercellular adhesions are required for the cell survival. ECM provides survival cues for many cell types (Meredith et al., 1993). To evaluate the role of ECM in this setting, we suspended the dissociated single cells in Matrigel and cultivated them as Matrigel/single cell clumps. The single cells in Matrigel also underwent apoptosis (Figure 2K), indicating that Matrigel/ECM was not sufficient for the survival of these single cells. When the dissociated cells were plated onto Matrigel-coated plates, some cells attached to the culture surface and grew, whereas others remained in suspensions and died, indicating the heterogeneity in forming cell-substrate adhesions (Figure 2L). In sum, Dispase-mediated cell detachment and subsequent floating culture led to differential cell survival in floating spheres, with the cell survival depending on intercellular adhesions.

Molecular characterization indicated that the folding cell sheets were enriched with polarized $VSX2^+$ RPCs and $PAX6^{high}$ progenitors. Upon the cell detachment, the original monolayer cell sheets remodeled to form layered cell sheets with a thickness of 6–8 cells via cell intercalation (Figures 3A–3I and S3A–S3C; n = 10/10, independent cell sheets). Interestingly, TJP1, PRKCZ, and CDH2 (also known as N-cadherin) were polarized to the surfaces of the cell sheets either predominantly to the concave surface (Figures 3A, 3G–3I; n = 7/10, independent sheets) or to both surfaces (Figure S3B, n = 3/10, independent sheets), indicating that TJs and AJs held the cell sheets together. Pulsed contractions of an actomyosin network likely regulate the apical constriction in the folding of neural tube (Karfunkel, 1972; Martin et al., 2009). In the folding cell sheets, pMYL2 (phosphorylated myosin light chain 2, also known as pMLC2) and F-actin were polarized to the surfaces of the cell sheets at various levels (Figures 3C, 5A, and S5A), suggesting that actomyosin-mediated contractions are the driving forces in the cell sheet folding. COL4A3 (collagen IV α3) was at convex surfaces and LAMB1 displayed a variable pattern (Figures 3A, 3H, and 3I). The cell sheets widely expressed PAX6 with a high level at the periphery and a moderate level at the center (Figures 3B and 3E; n = 3/10, independent sheets). $PAX6^{moderate}$ cells expressed VSX2 (Figures 3D and 3E), whereas $PAX6^{high}$ cells expressed MITF (Figures 3E and 3F). The pattern of $PAX6^{high}$ progenitors and $VSX2^+$ RPCs in the folding cell sheets was consistent with that in the monolayer sheets (compare Figures 3B, 3D, and 3E with Figures 1F and 1G), indicating that the patterning in $PAX6^{high}$ progenitors and $VSX2^+$ RPCs was largely maintained in the remodeling from the monolayer to the layered cell sheets.

In sum, Dispase-mediated cell detachment of the cyst-derived adherent cultures led to the isolation of $VSX2^+$ RPCs and $PAX6^{high}$ RPE progenitors as epithelial cell sheets via intercellular adhesion-dependent cell survival.

Self-Formation of Apically Convex $VSX2^+$ Epithelium

Live imaging and time-course immunohistochemistry of the spheres demonstrate self-formation of apically convex $VSX2^+$ epithelium in floating culture (Figures 3 and 4; Movie S2). After 14–16 hr of floating culture, TJP1 and PRKCZ became predominantly polarized to the convex surface and were downregulated at the concave surface. Furthermore, the cells close to the concave surface remodeled their intercellular adhesions to form rosettes with TJP1 and PRKCZ at lumens (Figures 3J and 3K; n = 4/4, independent aggregates). This pattern contrasted to that in the shortly detached cell sheets in which TJP1 and PRKCZ were either predominantly polarized to the concave surface or equally to both surfaces (Figures 3A, 3G, 3H, S3B, and S5B). After 2 days of floating culture, $VSX2^+$ RPCs near the convex surface of the spheres formed a layer of epithelium, whereas internal $VSX2^+$ RPCs began to self-organize into an epithelial layer with the opposite cell polarity. Abundant LAMB1 was found between the two cell layers, indicative of its involvement in cell epithelialization (Figures 3J–3M, 3O, S3E, and S3H). These results indicated that the structure of the initially detached $VSX2^+$ cell sheets with TJP1 and PRKCZ at the concave surface or both surfaces was transient and unstable; in 2 days, $VSX2^+$ RPCs spontaneously remodeled their intercellular adhesions to form two epithelial layers with opposite cell polarity; $VSX2^+$ RPCs eventually formed apically convex epithelium in floating culture. During this tissue morphogenesis, numerous cells underwent apoptosis and were shed off (Figures 3N, S3F, and S3I; Movie S2). The disintegrated cells lacked proper intercellular adhesions (Figure S5C, inset),

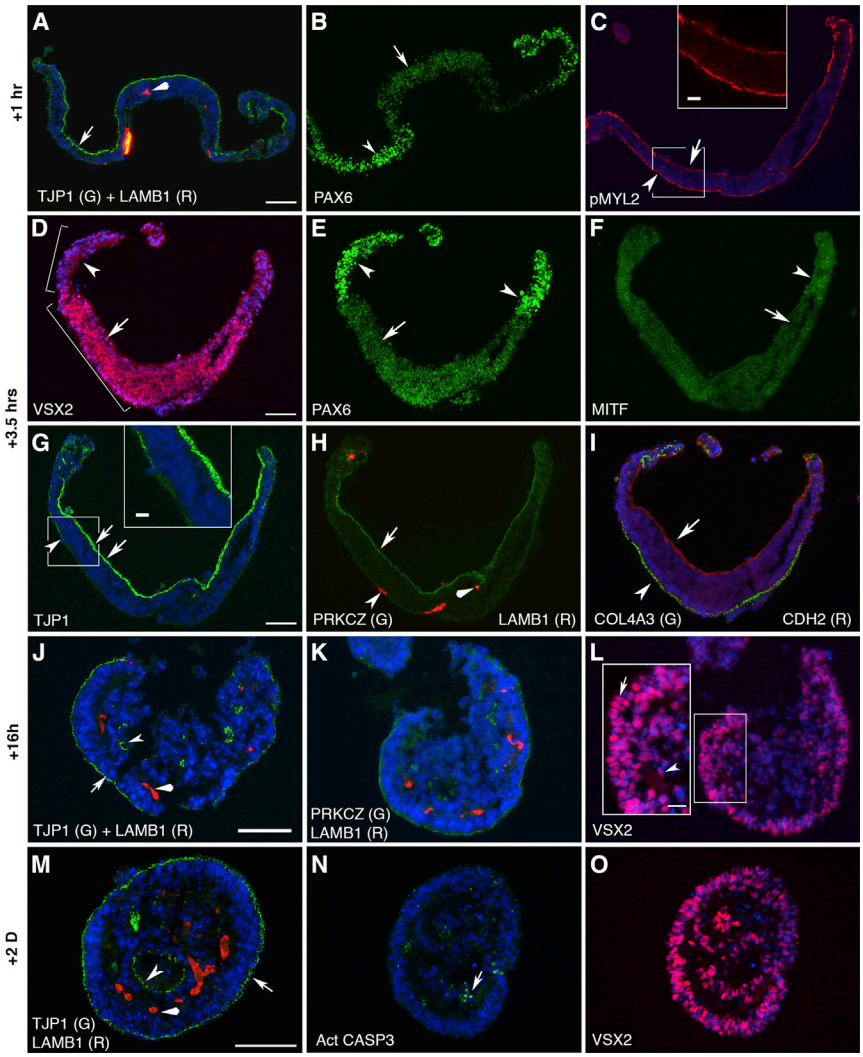

Figure 3. The Detached Cell Sheets Are Composed of Patterned VSX2$^+$ RPCs and PAX6^{high} RPE Progenitors and Remodel into Epithelial Layers in Floating Culture

(A–I) Immunostaining of the cell sheets at D13 + 1 hr and D13 + 3.5 hr (shown in Figures 2C and 2D). The cell sheets folded within hours, as revealed by TJP1 expression (arrows in A and G). TJP1 was predominantly at the concave (inner) surface (arrows, arrowhead, and inset in G). A pattern along the center-periphery axis was indicated by the expression of PAX6, VSX2, and MITF (arrows and arrowheads in B, D, E, and F). pMYL2 was polarized to the surfaces of the cell sheets at various levels (arrow, arrowhead, and inset in C), revealing a driving force in the folding. PRKCZ and CDH2 were at the concave surface (arrows in H and I), COL4A3 was at convex (outer) surface (arrowhead in I), and LAMB1 displayed a variable pattern (arrowhead and diamond arrowhead in A and H).

(J–O) Immunostaining of remodeling aggregates at D13 + 16 hr and D13 + 2D. At D13 + 16 hr, TJP1 (arrow in J) and PRKCZ (K) were mostly at the convex (outer) surface. A few rosettes with TJP1 (arrowhead in J) and PRKCZ (K) at lumens were found at areas close to the concave surface; VSX2$^+$ RPCs formed an epithelial layer at the convex surface (arrow in L), whereas VSX2$^+$ RPCs close to the concave surface were in the process of remodeling (arrowhead in L). At D13 + 2D, two epithelial layers of VSX2$^+$ RPCs with TJP1 at the apical surface (arrow and arrowhead in M and O) formed. LAMB1 was in between the layers (diamond arrowheads in J and M). Extensive apoptosis was found (arrow in N). Scale bars, 100 μm (A–O) and 20 μm (insets). See also Figure S3 and Movie S2.

confirming that intercellular adhesions are crucial for the differential cell survival.

The tissue remodeling in floating culture generated large quantities of distinguishable spheres (Figures 4A and 4B; 400–600 spheres per six-well plate of H1 hESCs, n > 10, independent experiments). Immunohistochemistry of spheres on D13 + 9D (i.e., 9 days of floating culture after cell detachment on day 13, 22 days of culture in total; similar abbreviations are used hereafter) revealed that VSX2 (Figure 4D, 90%) and SIX3 (Figure 4E) were highly expressed in the epithelium (n = 5/5, independent retinal organoids). The VSX2$^+$ epithelium moderately expressed PAX6, but rarely expressed OTX2 (Figures 4D, 4F, and 4G), a pattern that is reflective of RPC identity. In the area where VSX2 expression was low or absent, PAX6 and OTX2 were highly expressed (arrowheads in Figures 4F and 4G), a pattern representative of RPE progenitor identity. The pattern of VSX2$^+$ RPCs and PAX6^{high} RPE progenitors in the spheres was consistent with those in the previous stages (Figures 1F, 1G, 3B, and 3D–3F). The self-organized spheres are referred to as retinal organoids hereafter. Both TJP1 and PRKCZ were polarized to the outer (convex) surface of the retinal organoids (Figures 4H and 4I; compare with Figure 3G). A connecting stalk between the outer VSX2$^+$ epithelium and the inner VSX2$^+$ epithelium (diamond arrow in Figure 4I) indicated fusion of the two epithelial layers. The procedure described here for the generation of

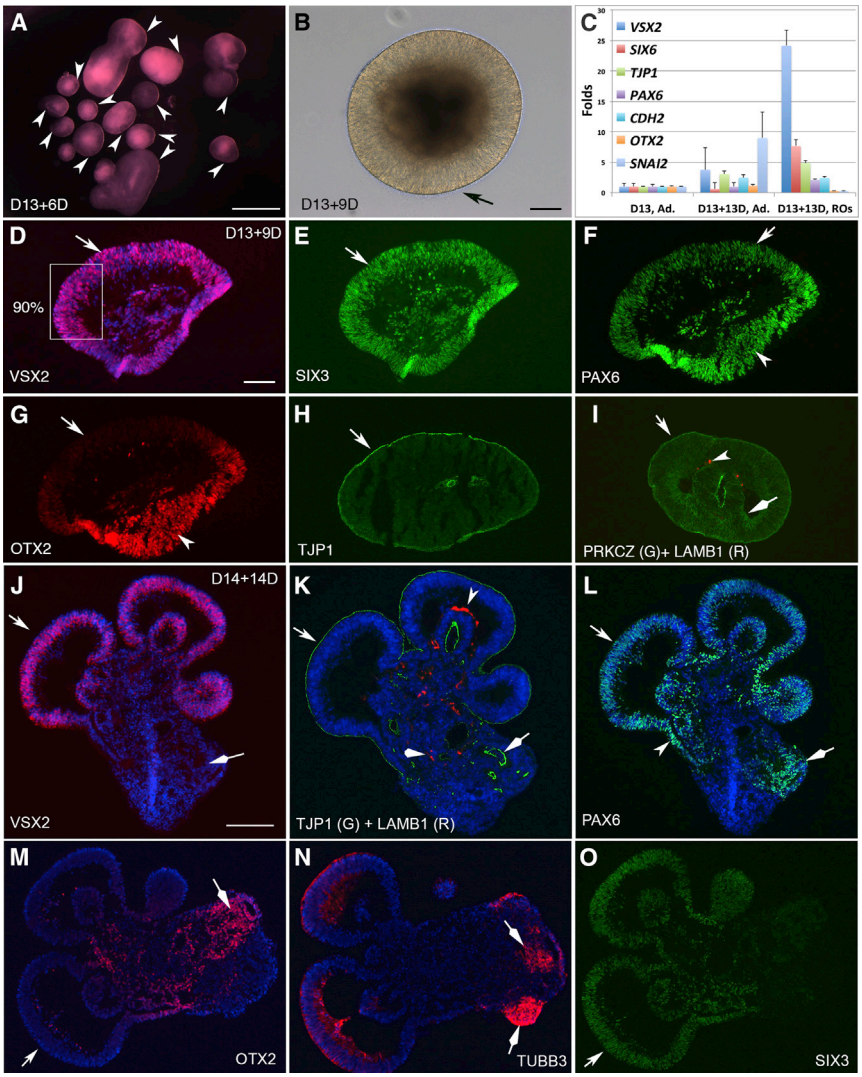

Figure 4. Self-formation of Retinal Organoids Comprising Apically Convex VSX2$^+$ Epithelium and PAX6^{high} RPE Progenitors in Floating Cultures

(A) Live view of retinal organoids at D13 + 6D. Note the translucent areas (arrowheads). 400–600 spheres per 6-well plate of H1 hESCs, n > 10 independent experiments.

(B) A high-magnification view of a D13 + 9D retinal organoid with a bright ring (arrow in B).

(C) RT-qPCR with RNA isolated from three individual wells of adherent cultures on D13, four individual wells of adherent cultures on D13 + 13D, and four groups of retinal organoids on D13 + 13D (15 pooled retinal organoids in each group). The expression was represented as fold changes relative to that in adherent cultures on D13. Mean ± SD of four or three individual wells of adherent cultures or groups of retinal organoids. Expression changes between D13 and D13 + 13D adherent cultures indicated cell differentiation in time course. Expression pattern in retinal organoids consistently differed from that in adherent cultures on D13 + 13D: the expression of VSX2, SIX6, and TJP1 was higher, but the expression of OTX2 and SNAI2 was lower. Ad., adherent cultures; ROs, retinal organoids.

(D–I) Immunostaining of the retinal organoid at D13 + 9D (B). VSX2 was highly expressed in the epithelium (D, 90%). VSX2$^+$ cells expressed SIX3 and PAX6, but not OTX2 (arrows in E–G). The peripheral cells with low or no VSX2 highly expressed PAX6 and OTX2 (arrowheads in F and G). TJP1 and PRKCZ were at the convex surface of VSX2$^+$ epithelium (arrows in H and I). LAMB1 expression was variable (arrowhead in I). A stalk connected the outer and inner epithelium (diamond arrow in I).

(J–O) VSX2$^+$ RPCs sorted out from OTX2$^+$ cells and self-organized into an apically convex epithelium in aggregates at D14 + 14D. VSX2 was specifically expressed in the epithelium with TJP1 at convex surface, whereas OTX2 was expressed in VSX2$^-$ regions with TJP1 at concave surface (lumens) (arrows and diamond arrows in J, K, and M). LAMB1 was found at the basal surface of internal VSX2$^+$ epithelium (arrowhead in K) and amorphous areas (diamond arrowhead in K). TUBB3 was expressed (diamond arrows in N). VSX2$^+$ RPCs co-expressed PAX6 and SIX3 (arrows in J, L, and O). Scale bars, 500 μm (A), 100 μm (B, D–I) and 200 μm (J–O). See also Figure S4 and Movie S2.

retinal organoids was validated in a line of hiPSCs (Figures S4G–S4L).

Analysis of fused retinal organoids, which resulted from a high seeding density of the cysts, demonstrated the self-organization of VSX2$^+$ epithelium more strikingly (Figures 4J–4O and S4A–S4F). In an aggregate with several fused retinal organoids on D14 + 14D, VSX2 was specifically expressed in the epithelium with TJP1 and PRKCZ at the outer (convex) surface (Figures 4J, 4K, S4B, S4E, and S4F), whereas OTX2 was expressed in VSX2$^-$ regions with TJP1 and PRKCZ at the luminal surface (concave surface) (Figures 4K and 4M). An internal VSX2$^+$ epithelium with the opposite cell polarity was fusing and flipping out (Figures 4J, 4K, and S4B–S4F). VSX2$^+$ epithelium moderately expressed PAX6 and SIX3, whereas peripheral VSX2$^-$ cells highly expressed PAX6 (Figures 4J, 4L, 4O, S4B, and S4C). In the VSX2$^+$ epithelium, cells expressing POU4F2 (BRN3) (data not shown) and OTX2 (Figure 4M) were

rare, indicating that neuronal differentiation in the retinal epithelium was still at its early stages similar to E11.5 in mice. In E10.5 mouse embryos, *OTX2* is expressed in midbrain, hindbrain, dorsal forebrain, and RPE; *PAX6* is expressed in midbrain, hindbrain, dorsal forebrain, spinal cord, RPE, and NR; *SIX3* is expressed in ventral forebrain, RPE, and NR (Gray et al., 2004). In the aggregates, VSX2$^-$ cells mostly expressed OTX2, PAX6, and TUBB3, indicative of cell identity of midbrain, hindbrain, and dorsal forebrain (Figures 4L–4O). These results indicate that VSX2$^+$ RPCs self-sorted out from OTX2$^+$ brain cells and organized into apically convex epithelium.

To quantify gene-expression changes in retinal organoid morphogenesis, we isolated RNA from adherent cultures on D13, adherent cultures on D13 + 13D, and retinal organoids on D13 + 13D for quantification using RT-qPCR (Figure 4C). In adherent cultures on D13 + 13D, the expression of VSX2, TJP1, CDH2, and SNAI2 (neural crest marker) (Sefton et al., 1998) increased compared with that on D13, indicating cell differentiation in time course. The high SD between different wells of adherent cultures on D13 + 13D reflects heterogeneity of the adherent cultures. Importantly, the expression pattern in retinal organoids consistently differed from that in adherent cultures on D13 + 13D: the expression of VSX2, SIX6, and TJP1 was higher, but the expression of OTX2 and SNAI2 was lower. The high VSX2 expression in retinal organoids revealed by RT-qPCR was consistent with the high abundance of VSX2$^+$ cells revealed by immunostaining (Figures 3, 4, S3, and S4).

In sum, Dispase-mediated cell detachment and subsequent floating culture led to enrichment of VSX2$^+$ RPCs and self-formation of apically convex VSX2$^+$ epithelium, forming retinal organoids.

Inhibition of ROCK or Myosin Activity Disrupts the Self-Organization of VSX2$^+$ Epithelium but Does Not Suppress Apoptosis

The polarized expression of TJP1, PRKCZ, CDH2, F-actin, and pMYL2 at the apical surface of the detached cell sheets and retinal organoids suggest the involvement of these proteins in retinal organoid morphogenesis (Figures 3, 4, S3, and S4). To determine whether ROCK-regulated actomyosin-driven forces are required, we supplemented myosin inhibitor blebbistatin and ROCK inhibitor Y27632 to the medium before, during, and after Dispase treatment. Y27632 delayed Dispase-mediated cell detachment (data not shown). In cell sheets 2 hr after the detachment, pMYL2 was polarized to the surfaces in the controls, but was downregulated or barely detectable in the blebbistatin- and Y27632-treated ones (Figures 5A–5C; n = 3/3, independent sheets). Consistently, F-actin, PRKCZ, and CDH2 were also significantly downregulated or barely detectable after Y27632 treatment (Figures S5A–S5F; n = 3/3, independent sheets), confirming the crucial roles of ROCK in the regulation of pMYL2, actin organization, cell polarity, and AJs (Amano et al., 2010). After 2 days of floating culture, VSX2$^+$ RPCs self-organized into two epithelial layers with opposite cell polarity in the controls, whereas the self-organization was not evident and TJP1 was downregulated in the blebbistatin- or Y27632-treated aggregates (Figures 5D–5I). In contrast, the apoptosis was unaffected (Figures 5J–5L; n = 4/4, independent aggregates; Movies S2 and S3). The effects of blebbistatin and Y27632 were more evident in retinal organoids on day 26, in which VSX2$^+$ cells failed to sort out and self-organize into apically convex epithelium (Figures 5M–5R and S5J–S5R; n = 4/4 for Y27632, n = 3/4 for blebbistatin, independent aggregates). The blebbistatin-treated aggregates contained deeply embedded vesicles with TJP1 and PRKCZ at the luminal surface, and displayed an irregular pattern of LAMB1 (Figures 5Q and S5N). In the Y27632-treated aggregates the expression of TJP1, PRKCZ, and LAMB1 was downregulated and displayed an irregular pattern (Figures 5R and S5O). Conversely, supplementing an antibody-neutralizing ITGB1 to the medium did not cause overt change (Figures S6A–S6H). Thus, ROCK-regulated actomyosin-driven forces are required for self-formation of the retinal organoids.

The Retinal Organoids Generate NR with Outer Segments, CM, and RPE

To evaluate the developmental potential of the retinal organoids, we analyzed them in long-term cultures. On day 54, retinal organoids displayed patterned NR, CM, and RPE as revealed by the following markers: VSX2 for RPCs, PAX6 for RPCs and differentiating amacrine cells, OTX2 for differentiating photoreceptors, bipolar cells, and horizontal cells, ISL1/2 and POU4F2 for ganglion cells, TUBB3 for ganglion cells and amacrine cells, RCVRN for photoreceptors, PRKCZ for apical polarity, OTX2 and MITF for RPE, and FUT4 (SSEA-1) and RDH10 for CM (Kuwahara et al., 2015) (Figures 6A–6L, S6K, and S6L). The misplacement of RPE in retinal organoids is explained by the lack of forces holding the ends of RPE sheets at the back in the formation of apically convex VSX2$^+$ epithelium (Figures 3A–3I). On day 152, retinal organoids maintained stratified structure and expressed the major markers: VSX2$^+$ PAX6$^+$ for RPCs, VSX2$^-$ PAX6$^+$ for amacrine cells, VSX2$^+$ PAX6$^-$ for bipolar cells, RCVRN$^+$ OTX2$^+$ for photoreceptors, RCVRN$^-$ OTX2$^+$ for bipolar and horizontal cells, and RHO for rod photoreceptors (Figures 6M–6O). Occasionally, self-organized retinal organoids formed in adherent cultures (Figures S6M–S6O). Importantly, retinal organoids on day 187 exhibited dense cilia (n = 50/67, independent retinal organoids), highly expressed RHO, OPN1LW/OPN1MW, and

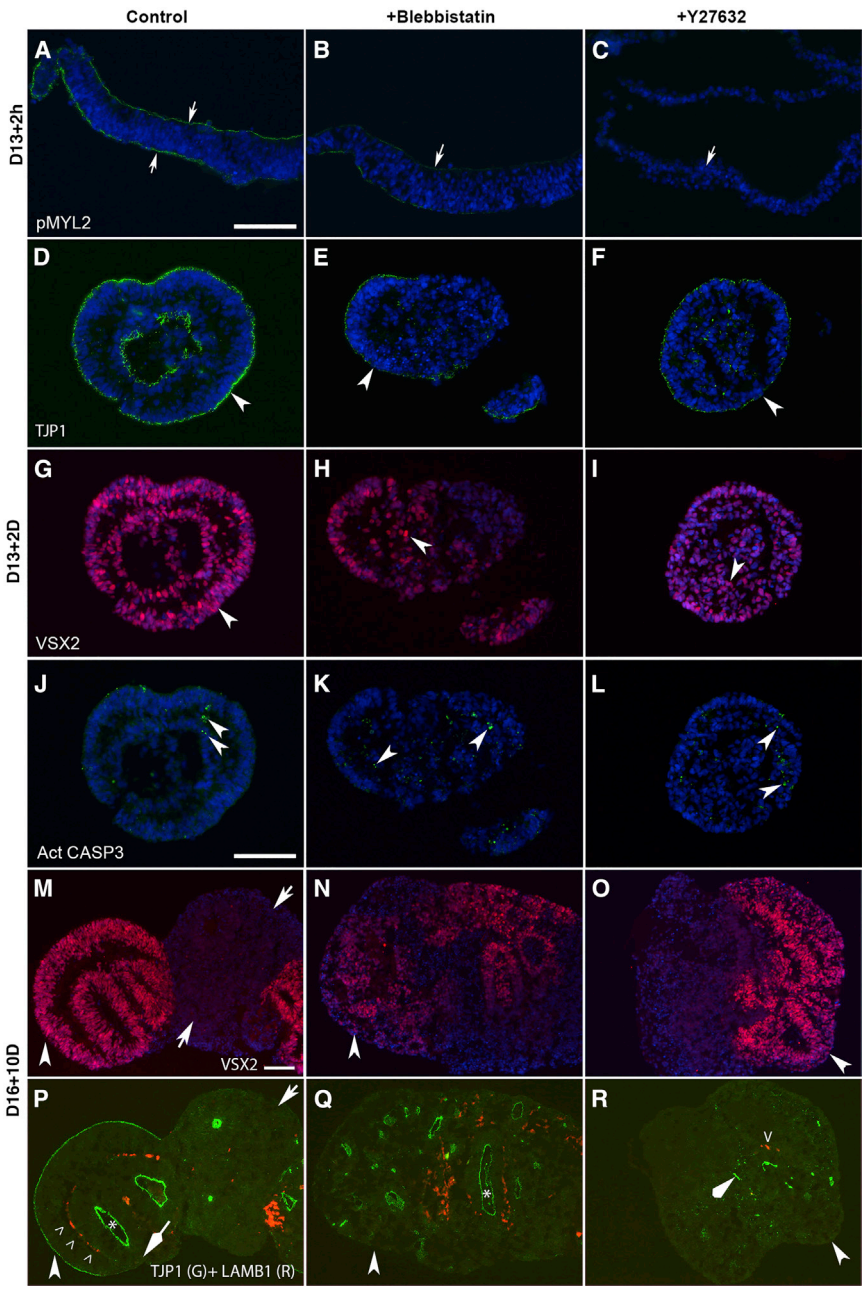

Figure 5. Inhibition of Myosin and ROCK Activity Disrupts the Self-Organization of Apically Convex VSX2$^+$ Epithelium but Does Not Affect the Apoptosis

(A–R) Myosin inhibitor blebbistatin (50 μM) and ROCK inhibitor Y27632 (10 μM) were supplemented to the medium 1 hr before, during, and following the cell detachment for the time as indicated. After blebbistatin or Y27632 treatment, pMYL2 was reduced or undetectable (arrows in A–C) at D13 + 2 hr; at D13 + 2D, TJP1 was reduced (arrowheads in D–F), VSX2$^+$ epithelium was less evident or absent (arrowheads in G–I), but activated CASP3 (act CASP3) was unaffected (arrowheads in J–L) (n = 4/4, independent aggregates). At D16 + 10D, VSX2$^+$ cells failed to sort out and self-organize to form apically convex epithelium after blebbistatin or Y27632 treatment (arrowheads in M–R; n = 4/4 for Y27632, n = 3/4 for blebbistatin, independent aggregates). In the control, VSX2$^+$ RPCs formed apically convex epithelium (arrowheads in M and P), whereas VSX2$^-$ cells were not (arrows in M and P). An internal VSX2$^+$ epithelium with TJP1 at the lumen (* in P) deposited LAMB1 at the basal surface (^ in P). The fusing region lacked TJP1 at the outer surface (diamond arrow in P). In the blebbistatin-treated aggregates, TJP1 was at luminal surfaces of internal vesicles (* in Q). In the Y27632-treated aggregates, TJP1 expression was reduced and irregular (diamond arrowhead in R); LAMB1 pattern was irregular (^ in R). Scale bars, 100 μm. See also Figure S5 and Movie S3.

OPN1SW, and displayed the ultrastructure of outer segments, i.e., enriched mitochondria, outer limiting membrane, connecting cilia, basal bodies, centrioles, and membrane discs (Figure 7), indicating the maturation of photoreceptors in retinal organoids. The membrane discs in retinal organoids mimicked the differentiating outer segments in mice (Obata and Usukura, 1992). The presence of cilia correlated with high expression of RHO, OPN1LW/OPN1MW, and OPN1SW (n = 3/3, independent retinal organoids). Retinal organoids expressed the major markers for NR and RPE (Figure S7). In sum, the retinal organoids in long-term cultures generated a retinal tissue comprising NR, CM, and RPE.

DISCUSSION

With a culture system established here, we dissected retinal organoid morphogenesis in hESC-derived cultures. We demonstrate that intercellular adhesion-dependent cell survival and ROCK-regulated actomyosin-driven forces are required for self-formation of retinal organoids and

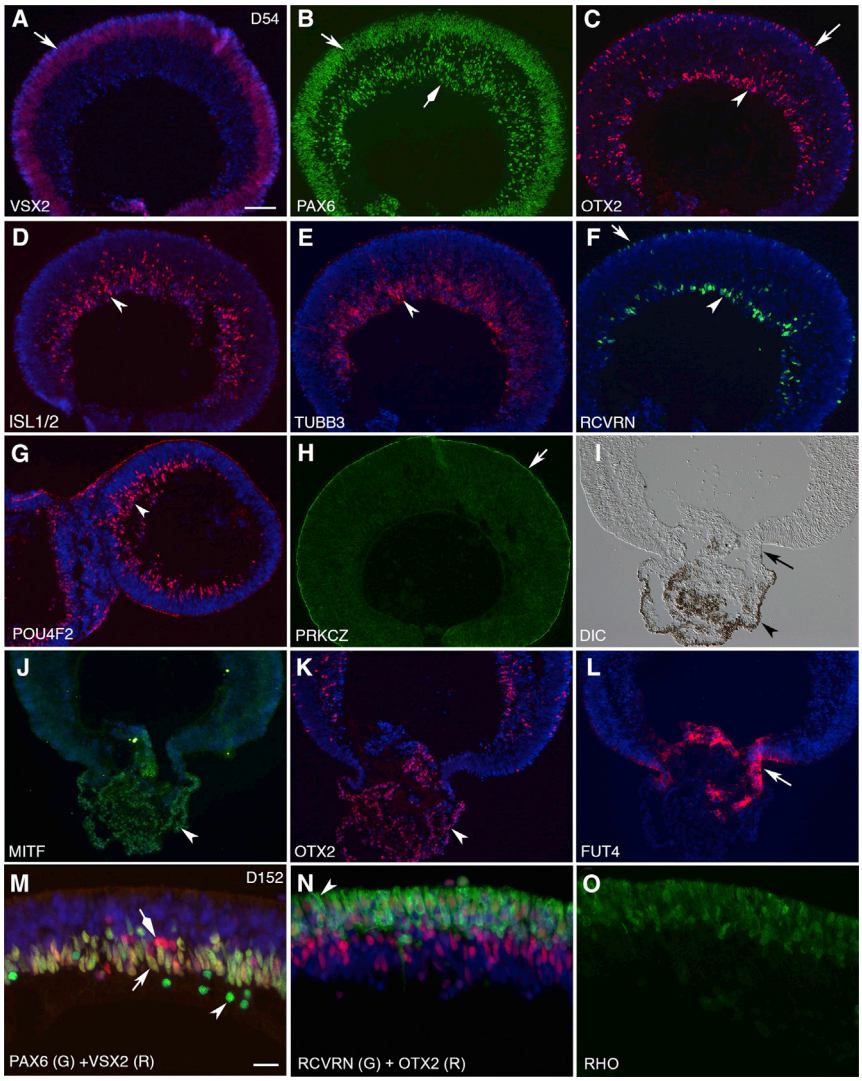

Figure 6. The Retinal Organoids Generate Stratified NR, CM and RPE

(A–O) Immunohistochemistry of retinal organoids on day 54 (A–L) and day 152 (M–O). The stratified NR expressed the major markers for retinal cells: VSX2, RPCs (arrow in A); PAX6, RPCs, amacrine cells (arrow and diamond arrow in B, respectively); OTX2, photoreceptors, bipolar cells, horizontal cells (arrow and arrowhead in C); ISL1/2, ganglion cells (arrowhead in D); TUBB3, ganglion cells, amacrine cells (arrowhead in E); RCVRN, photoreceptors (arrow and arrowhead in F); POU4F2, ganglion cells (arrowhead in G); PRKCZ, apical marker (arrow in H); MITF, RPE (arrowhead in J); OTX2, RPE (arrowheads in K and I); FUT4, CM (arrows in I and L); $VSX2^{+}$ $PAX6^{+}$, RPCs (arrow in M); $VSX2^{-}$ $PAX6^{+}$, amacrine (arrowhead in M); $VSX2^{+}$ $PAX6^{-}$, bipolar (diamond arrow in M); $OTX2^{+}$ $RCVRN^{+}$, photoreceptors (N; apical protrusion is indicated by arrowhead); $OTX2^{+}$ $RCVRN^{-}$, bipolar and horizontal (N); RHO, rod photoreceptors (O).

Scale bars, 100 μm (A–L) and 20 μm (M–O). See also Figure S6.

propose a hypothesis that newly specified $VSX2^{+}$ RPCs form characteristic structures in equilibrium via minimization of cell surface tension. Our Dispase-mediated method is convenient for isolation of large amounts of optic cup-like retinal organoids with minimal manual manipulation, has been validated in two lines of hPSCs, and differs substantially from the methods of manual dissection or mechanical scraping described previously (Meyer et al., 2009, 2011; Nakano et al., 2012; Reichman et al., 2014; Zhong et al., 2014). The retinal organoids autonomously generate stratified retinal tissues with all retinal cell types in cultures, and thus are powerful models for studying human retinal development and disease.

The ECM provides cues for coordinated cell polarization and cell survival in the transformation from the initially amorphous epiblast into the cup-shaped epithelium in mouse blastocysts (Bedzhov and Zernicka-Goetz, 2014; Coucouvanis and Martin, 1995). It also underlies cell epithelialization of the eye field in zebrafish (Ivanovitch et al., 2013). Matrigel (56% laminin, 31% collagen IV, and 8% entactin), an ECM surrogate, is used in retinal differentiation by either being suspended in culture media (Boucherie et al., 2013; Nakano et al., 2012) or forming a solidified layer of Matrigel/cells onto culture surfaces (Zhu et al., 2013). Here, floating culture of Matrigel/hESC clumps generates epithelialized cysts. In our hands, cell epithelialization is more efficient via Matrigel-aided cyst formation than by culturing embryonic bodies in Matrigel-containing media. In contrast to the solidified layer on culture surfaces (Zhu et al., 2013), the floating clumps of Matrigel/hESCs described here permit the cells to have better access to medium, and cysts in the floating clumps spontaneously attach to culture surfaces and spread at later stages. Matrigel promotes cell survival and epithelialization in cyst

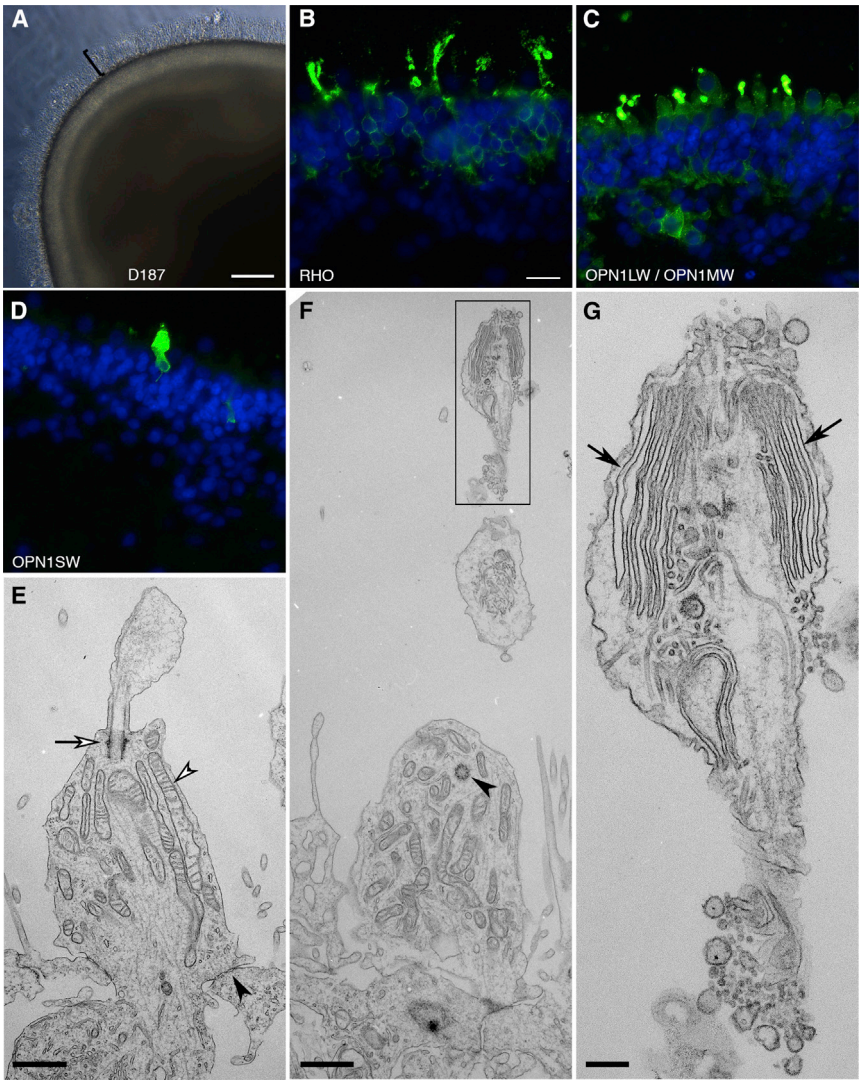

Figure 7. The Ultrastructure of Outer Segments in the Photoreceptors

(A–G) Retinal organoids at month 6 displayed dense cilia (bracket in A, n = 50/67, independent retinal organoids), highly expressed RHO, OPN1LW/OPN1MW, and OPN1SW (B–D), and exhibited the ultrastructure of outer segments (E–G): basal bodies, mitochondria, outer limiting membrane (open arrow, open arrowhead, and arrowhead in E), basal bodies (arrowhead in F), and membrane discs (arrows in G).

Scale bars, 100 μm (A), 20 μm (B–D), 1 μm (E and F), and 0.2 μm (G). See also Figure S7.

formation likely through integrin signaling (Manninen, 2015). In addition, epithelial structure of the cysts could confer cell survival, since correct polarization of acini accounts for resistance to apoptosis in breast cancer cell lines (Weigelt and Bissell, 2008). In literature, inhibitors of ROCK or myosin are used in retinal differentiation to suppress undesirable apoptosis (Nakano et al., 2012; Zhong et al., 2014). It is possible, however, that the inhibition compromises cell epithelialization. In our system, ROCK inhibitor Y27632 is dispensable and disruptive in cyst formation. Spontaneous cell specification in the epithelialized cysts from the initial pluripotent fate to the cell fates of anterior ectoderm/neural plate, eye field, and optic vesicle resembles neural differentiation as default (Stern, 2006); the existence of both retinal cells and brain cells in the cultures reflects the multipotency and/or heterogeneity of the cysts. We conclude that 3D contact between Matrigel and small hESC sheets provides a cue similar to that in the blastocyst and the eye field, leading to efficient epithelialization of hESCs and retinal differentiation.

The in vitro process of spontaneous attachment and spreading of the cysts, Dispase-mediated detachment, and subsequent floating culture achieves an outcome similar to that in in vivo optic cup invagination from optic vesicles. A process of embryonic body formation, attachment, manual dissection or mechanical scraping, and floating culture was described previously (Meyer et al., 2009, 2011). Cysts are epithelial structures, whereas embryonic bodies are amorphous solid cell masses. Similar to optic vesicles, cysts are apically concave and express optic vesicle markers. However, cysts do not invaginate properly, but later become disorganized and spontaneously attach to culture surfaces. Disorganization of the cysts can be explained by uncoordinated morphogenesis in closed-ended

cysts. Spontaneous attachment and spreading of the cysts, however, led to a morphogenetic change from closed-ended cysts to open-ended epithelial monolayer sheets comprising patterned VSX2$^+$ RPCs and PAX6^{high} RPE progenitors. Remodeling of intercellular adhesions, coordinated cell movements, regulation of cell surface tension, and cell differentiation and proliferation contribute to the patterning. Consistent with center-periphery patterning of VSX2$^+$ RPCs and PAX6^{high} progenitors described here, concentric patterning of ocular cells was recently described (Hayashi et al., 2016). In contrast, when the cysts are dissociated into single cells and passaged, no overt pattern is observed in VSX2$^+$ RPCs (Zhu et al., 2013). We conclude that spontaneous attachment and spreading of the cysts lead to the formation of patterned epithelial monolayer sheets of VSX2$^+$ RPCs and PAX6^{high} progenitors in the adherent cultures.

Dispase-mediated detachment allows us to dissect morphogenetic events that were not probed previously. The detachment disrupted ECM-cell adhesions and induced polarization of pMYL2, F-actin, TJP1, PRKCZ, and CDH2 to the surfaces of cell sheets. The spontaneous remodeling from monolayer sheets of VSX2$^+$ RPCs to stratified sheets upon the detachment resembles in vivo epithelial intercalation via cell-junction remodeling driven by local regulation of intercellular surface tension (Lecuit and Lenne, 2007). In subsequent floating culture, differential cell survival and spontaneous tissue remodeling led to cell sorting and self-formation of retinal organoids, reflecting an intrinsic property of VSX2$^+$ RPCs. We determine that the cell survival relies on Ca^{2+}-dependent intercellular adhesions, because (1) CDH2 and TJP1 held the cell sheets at the apical surface; (2) EGTA disintegrated the cell sheets, and EGTA-mediated Ca^{2+} chelation leads to the disassembly of TJP1 and E-cadherin in MDCK cells (Rothen-Rutishauser et al., 2002); (3) the cells became disintegrated when they lost intercellular adhesions; and (4) the cell survival was lost when the cell sheets were dissociated. In the literature, E-cadherin, CDH2, and TJP1 regulate cell growth and survival (Katsuno et al., 2008; Oliver et al., 2013; Wheelock et al., 2008). In self-formation of retinal organoids, intercellular adhesions are required for differential cell survival, although the specific role of TJP1 and CDH2 remains to be determined.

In the detached cell sheets, retinal progenitors have substantial freedom in forming a structure in equilibrium, whereas they have to overcome anchorage forces in adherent cultures or inside embryonic bodies. According to the cell surface tension model, cells with the same adhesion properties in a tissue tend to aggregate in clusters in equilibrium via coordinated forces generated by intercellular adhesions and ROCK-regulated actomyosin-driven cortical tension so that the surface area of contact with the surrounding environment is reduced and the intercellular surface tension is minimized (Lecuit and Lenne, 2007; Steinberg, 1963). Our findings are in line with this model and support a hypothesis that, in a constraint-free environment, cell-specific intercellular adhesions in newly specified VSX2$^+$ RPCs lead to cell sorting and self-organization of an apically convex epithelium in equilibrium so that cell surface tension is minimized. The supportive findings are: (1) self-organization of apically convex VSX2$^+$ epithelium (retinal organoids) occurred spontaneously and reproducibly in floating culture in which physical constraints are minimized; (2) in fused retinal organoids, VSX2$^+$ RPCs (with TJP1 and PRKCZ at the convex surface) self-sorted out from OTX2$^+$ embryonic brain cells (with TJP1 and PRKCZ at the lumens); (3) LAMB1 was assembled at the basal surface in the epithelialization; (4) retinal organoids formed spontaneously but at a much lower frequency in adherent culture in which anchorage forces constrained morphogenesis; (5) intercellular adhesions were remodeled during self-organization of retinal organoids; (6) ROCK-regulated actomyosin-driven forces mediated the morphogenesis (see below); and (7) optic cup invagination in mouse coincides with changes in cell surface properties and transcription: peak levels of TJP1, PRKCZ, LAMB1, and VSX2 at E10.5. Our hypothesis explains the self-formation of retinal organoids described here, retinal structures described by others (Nakano et al., 2012; Reichman et al., 2014; Zhong et al., 2014), and VSX2$^+$ rosette structures when VSX2$^+$ cells are intermingled with other cells. If the hypothesis is correct, optic cup invagination in vivo represents the formation of equilibrium. Identification of cell-specific adhesion molecule(s) in VSX2$^+$ RPCs mediating the self-organization and examination of the cell surface tension will prove the hypothesis.

Forces generated by actomyosin networks within cells and forces transmitted through intercellular adhesions are coordinated in driving self-organized tissue morphogenesis (Heisenberg and Bellaiche, 2013). We determine that retinal organoid morphogenesis is mediated by ROCK-regulated actomyosin-driven forces, based on the evidence that (1) pMYL2 and F-actin were polarized to the surfaces of cell sheets upon Dispase-mediated detachment; (2) inhibition of ROCK significantly downregulated or abolished the polarized expression of pMYL2, F-actin, TJP1, PRKCZ, and CDH2; and (3) myosin inhibitor blebbistatin or ROCK inhibitor Y27632 disrupted the self-organization of apically convex VSX2$^+$ epithelium. ROCK exerted its roles during Dispase treatment, since a few retinal organoids still formed when Y27632 was added after Dispase treatment. In chick, Y27632 disrupts the invagination of optic vesicles as well as lens placode (Plageman et al., 2011), but it is unclear whether the phenotype in optic vesicles is directly caused by ROCK inhibition or indirectly by

defective lens morphogenesis. In contrast to our findings described here and those of Plageman et al. (2011) in the chick, the spontaneous apical eversion of hESC-derived NR was not affected by ROCK inhibitor, but was disrupted by an antibody-neutralizing integrin signaling (Nakano et al., 2012). The eversion of mESC-derived NR showed phase-specific dependence on ROCK activity (Eiraku et al., 2011). Live imaging and molecular characterization demonstrate that retinal organoid morphogenesis described here differs from the apical eversion of hESC-derived NR (Nakano et al., 2012), which explains the difference in ROCK dependence. We conclude that ROCK-regulated actomyosin-driven forces are required for self-formation of the retinal organoids.

The retinal organoids in cultures autonomously generated stratified retinal tissues. The findings described here and by others (Meyer et al., 2011; Reichman et al., 2014; Zhong et al., 2014) indicate that substantially pure $VSX2^+$ epithelium has an intrinsic property to differentiate into stratified NR. Although outer segments were recently described (Zhong et al., 2014), there is still an unmet need for generating more mature outer segments. The retinal differentiation system established here for generating photoreceptors with maturing outer segments has multiple applications in modeling human retinal development and disease.

EXPERIMENTAL PROCEDURES

Maintenance of hESCs

The Embryonic Stem Cell Research Oversight Committee and the Institutional Review Board committees at Albert Einstein College of Medicine approved the project. Undifferentiated H1 hESCs or hiPSCs were maintained with feeder-free methods.

Retinal Differentiation

Small cell sheets of undifferentiated H1 hESCs or hiPSCs were suspended in Matrigel for gelification, and the gel was gently dispersed into small clumps for floating culture, with cysts visible on day 1. On day 5 the cysts were transferred to new 24-well plates, 20–40 cysts per well. The cysts spontaneously attached to the culture surface, spread, and became adherent cultures. At a time point during days 12–17, the adherent cultures were detached as cell sheets with Dispase. The cell sheets were rinsed, then grown as floating structures and for long-term culture 2 weeks later.

Inhibition of Myosin and ROCK

Blebbistatin (50 μM) and Y27632 (10 μM) were added to the culture medium 1 hr before and during Dispase treatment, and during the culture.

SUPPLEMENTAL INFORMATION

Supplemental Information includes Supplemental Experimental Procedures, seven figures, and three movies and can be found with this article online at http://dx.doi.org/10.1016/j.stemcr.2016.03.011.

ACKNOWLEDGMENTS

We are thankful to Dr. R. Chuck for support, E. Bouhassira and HPSC Core in MRG Stem Cell Institute (supported by NYSTEM C029154 to P. Frenette) and AIF at AECOM for service, and Drs. J. Nathans and M. Redmond for antibodies. Grants were provided by BrightFocus (M2012044 to W.L.), NEI (1R01EY022645 to W.L., R01EY012200, R01EY014237 and R21EY020621 to A.C.), RPB (unrestricted), Joseph Alexander Foundation (to R. Chuck), T32GM007491 (A.L.), T32GM007288 (R.H.), and K12GM102779 (P.B).

Received: February 24, 2016
Revised: March 30, 2016
Accepted: March 31, 2016
Published: April 28, 2016

REFERENCES

Amano, M., Nakayama, M., and Kaibuchi, K. (2010). Rho-kinase/ROCK: a key regulator of the cytoskeleton and cell polarity. Cytoskeleton (Hoboken) *67*, 545–554.

Bedzhov, I., and Zernicka-Goetz, M. (2014). Self-organizing properties of mouse pluripotent cells initiate morphogenesis upon implantation. Cell *156*, 1032–1044.

Beysens, D.A., Forgacs, G., and Glazier, J.A. (2000). Cell sorting is analogous to phase ordering in fluids. Proc. Natl. Acad. Sci. USA *97*, 9467–9471.

Boucherie, C., Mukherjee, S., Henckaerts, E., Thrasher, A.J., Sowden, J.C., and Ali, R.R. (2013). Brief report: self-organizing neuroepithelium from human pluripotent stem cells facilitates derivation of photoreceptors. Stem Cells *31*, 408–414.

Coucouvanis, E., and Martin, G.R. (1995). Signals for death and survival: a two-step mechanism for cavitation in the vertebrate embryo. Cell *83*, 279–287.

Eiraku, M., Takata, N., Ishibashi, H., Kawada, M., Sakakura, E., Okuda, S., Sekiguchi, K., Adachi, T., and Sasai, Y. (2011). Self-organizing optic-cup morphogenesis in three-dimensional culture. Nature *472*, 51–56.

Frisch, S.M., and Francis, H. (1994). Disruption of epithelial cell-matrix interactions induces apoptosis. J. Cell Biol. *124*, 619–626.

Gray, P.A., Fu, H., Luo, P., Zhao, Q., Yu, J., Ferrari, A., Tenzen, T., Yuk, D.I., Tsung, E.F., Cai, Z., et al. (2004). Mouse brain organization revealed through direct genome-scale TF expression analysis. Science *306*, 2255–2257.

Hayashi, R., Ishikawa, Y., Sasamoto, Y., Katori, R., Nomura, N., Ichikawa, T., Araki, S., Soma, T., Kawasaki, S., Sekiguchi, K., et al. (2016). Co-ordinated ocular development from human iPS cells and recovery of corneal function. Nature *531*, 376–380.

Heisenberg, C.P., and Bellaiche, Y. (2013). Forces in tissue morphogenesis and patterning. Cell *153*, 948–962.

Ivanovitch, K., Cavodeassi, F., and Wilson, S.W. (2013). Precocious acquisition of neuroepithelial character in the eye field underlies the onset of eye morphogenesis. Dev. Cell. *27*, 293–305.

Jockusch, B.M., Bubeck, P., Giehl, K., Kroemker, M., Moschner, J., Rothkegel, M., Rudiger, M., Schluter, K., Stanke, G., and Winkler, J. (1995). The molecular architecture of focal adhesions. Annu. Rev. Cell Dev. Biol. *11*, 379–416.

Karfunkel, P. (1972). The activity of microtubules and microfilaments in neurulation in the chick. J. Exp. Zool. *181*, 289–301.

Katsuno, T., Umeda, K., Matsui, T., Hata, M., Tamura, A., Itoh, M., Takeuchi, K., Fujimori, T., Nabeshima, Y., Noda, T., et al. (2008). Deficiency of zonula occludens-1 causes embryonic lethal phenotype associated with defected yolk sac angiogenesis and apoptosis of embryonic cells. Mol. Biol. Cell *19*, 2465–2475.

Kuwahara, A., Ozone, C., Nakano, T., Saito, K., Eiraku, M., and Sasai, Y. (2015). Generation of a ciliary margin-like stem cell niche from self-organizing human retinal tissue. Nat. Commun. *6*, 6286.

Lamba, D.A., Gust, J., and Reh, T.A. (2009). Transplantation of human embryonic stem cell-derived photoreceptors restores some visual function in Crx-deficient mice. Cell Stem Cell *4*, 73–79.

Lancaster, M.A., and Knoblich, J.A. (2014). Organogenesis in a dish: modeling development and disease using organoid technologies. Science *345*, 1247125.

Lecuit, T., and Lenne, P.F. (2007). Cell surface mechanics and the control of cell shape, tissue patterns and morphogenesis. Nat. Rev. Mol. Cell Biol. *8*, 633–644.

Liu, W., Lagutin, O., Swindell, E., Jamrich, M., and Oliver, G. (2010). Neuroretina specification in mouse embryos requires Six3-mediated suppression of Wnt8b in the anterior neural plate. J. Clin. Invest. *120*, 3568–3577.

Manninen, A. (2015). Epithelial polarity—generating and integrating signals from the ECM with integrins. Exp. Cell Res. *334*, 337–349.

Martin, A.C., Kaschube, M., and Wieschaus, E.F. (2009). Pulsed contractions of an actin-myosin network drive apical constriction. Nature *457*, 495–499.

Meredith, J.E., Jr., Fazeli, B., and Schwartz, M.A. (1993). The extracellular matrix as a cell survival factor. Mol. Biol. Cell *4*, 953–961.

Meyer, J.S., Shearer, R.L., Capowski, E.E., Wright, L.S., Wallace, K.A., McMillan, E.L., Zhang, S.C., and Gamm, D.M. (2009). Modeling early retinal development with human embryonic and induced pluripotent stem cells. Proc. Natl. Acad. Sci. USA *106*, 16698–16703.

Meyer, J.S., Howden, S.E., Wallace, K.A., Verhoeven, A.D., Wright, L.S., Capowski, E.E., Pinilla, I., Martin, J.M., Tian, S., Stewart, R., et al. (2011). Optic vesicle-like structures derived from human pluripotent stem cells facilitate a customized approach to retinal disease treatment. Stem Cells *29*, 1206–1218.

Nakano, T., Ando, S., Takata, N., Kawada, M., Muguruma, K., Sekiguchi, K., Saito, K., Yonemura, S., Eiraku, M., and Sasai, Y. (2012). Self-formation of optic cups and storable stratified neural retina from human ESCs. Cell Stem Cell *10*, 771–785.

Obata, S., and Usukura, J. (1992). Morphogenesis of the photoreceptor outer segment during postnatal development in the mouse (BALB/c) retina. Cell Tissue Res. *269*, 39–48.

Oliver, C., Gonzalez, C.A., Alvial, G., Flores, C.A., Rodriguez, E.M., and Batiz, L.F. (2013). Disruption of CDH2/N-cadherin-based adherens junctions leads to apoptosis of ependymal cells and denudation of brain ventricular walls. J. Neuropathol. Exp. Neurol. *72*, 846–860.

Plageman, T.F., Jr., Chauhan, B.K., Yang, C., Jaudon, F., Shang, X., Zheng, Y., Lou, M., Debant, A., Hildebrand, J.D., and Lang, R.A. (2011). A Trio-RhoA-Shroom3 pathway is required for apical constriction and epithelial invagination. Development *138*, 5177–5188.

Reichman, S., Terray, A., Slembrouck, A., Nanteau, C., Orieux, G., Habeler, W., Nandrot, E.F., Sahel, J.A., Monville, C., and Goureau, O. (2014). From confluent human iPS cells to self-forming neural retina and retinal pigmented epithelium. Proc. Natl. Acad. Sci. USA *111*, 8518–8523.

Rothen-Rutishauser, B., Riesen, F.K., Braun, A., Gunthert, M., and Wunderli-Allenspach, H. (2002). Dynamics of tight and adherens junctions under EGTA treatment. J. Membr. Biol. *188*, 151–162.

Sefton, M., Sanchez, S., and Nieto, M.A. (1998). Conserved and divergent roles for members of the Snail family of transcription factors in the chick and mouse embryo. Development *125*, 3111–3121.

Steinberg, M.S. (1963). Reconstruction of tissues by dissociated cells. Some morphogenetic tissue movements and the sorting out of embryonic cells may have a common explanation. Science *141*, 401–408.

Stern, C.D. (2006). Neural induction: 10 years on since the 'default model'. Curr. Opin. Cell Biol. *18*, 692–697.

Weigelt, B., and Bissell, M.J. (2008). Unraveling the microenvironmental influences on the normal mammary gland and breast cancer. Semin. Cancer Biol. *18*, 311–321.

Wheelock, M.J., Shintani, Y., Maeda, M., Fukumoto, Y., and Johnson, K.R. (2008). Cadherin switching. J. Cell Sci. *121*, 727–735.

Zhong, X., Gutierrez, C., Xue, T., Hampton, C., Vergara, M.N., Cao, L.H., Peters, A., Park, T.S., Zambidis, E.T., Meyer, J.S., et al. (2014). Generation of three-dimensional retinal tissue with functional photoreceptors from human iPSCs. Nat. Commun. *5*, 4047.

Zhu, Y., Carido, M., Meinhardt, A., Kurth, T., Karl, M.O., Ader, M., and Tanaka, E.M. (2013). Three-dimensional neuroepithelial culture from human embryonic stem cells and its use for quantitative conversion to retinal pigment epithelium. PLoS One *8*, e54552.